Applied Soft Computing Journal 79 (2019) 341–353

Contents lists available at ScienceDirect

Applied Soft Computing Journal

journal homepage: www.elsevier.com/locate/asoc

High-speed fault detection and location in DC microgrids systems using Multi-Criterion System and neural network☆

Ali Abdali, Kazem Mazlumi *, Reza Noroozian

Department of Electrical Engineering, Faculty of Engineering, University of Zanjan, P.O. Box: 45371-38791, Zanjan, Iran

HIGHLIGHTS

- Protection of DC microgrid is highly challenging, unlike conventional AC system.
- A novel protection scheme based on MCS is proposed for DC microgrids.
- An accurate fault location scheme based on NN is presented for DC microgrids.
- The MCS, NN schemes and simulated network is implemented in laboratory-scale.
- MCS implementation leads to the reduction of the protective system cost.

ARTICLE INFO

Article history:
Received 18 February 2018
Received in revised form 12 February 2019
Accepted 30 March 2019
Available online 8 April 2019

Keywords:
Fault detection
Fault location
Multi-Criterion System (MCS)
Neural network (NN)
LVDC microgrids
Circuit breaker

ABSTRACT

This paper presents a new protection method for LVDC ring-bus microgrid systems based on Multi-Criterion System (MCS) and Neural Network (NN). The proposed method aimed at high-speed detecting line-to-ground (LG) and line-to-line (LL) low impedance faults without using a definite threshold of differential current by using specific rules and multi-criterion system. MCS protection showed speed and accuracy compared to differential protection. Also, NN estimated fault location in percent of line length acceptably as a secondary controller. In order to evaluate the reliability and the enforceability of fault detection and location schemes, simulated network and protection algorithms are implemented and tested in laboratory-scale. The implementation results indicate that the MCS and NN protection scheme can consistently detect and estimate fault locations in the order of a few milliseconds. To reach this goal, a loop type LVDC microgrid with proper power electronic equipment like solid-state bidirectional breakers and the multi-level inverter is fulfilled.

1. Introduction

DC microgrids are effective structure and solution to attain a reliable power with higher yield via the use of distributed generations (DGs) units, power electronics converters, and energy storage devices. As well as, DC microgrid is a practical solution for electric power distribution in various equipment like telecommunication systems, ships, spacecraft and distribution systems, which incorporate a considerable quantity of electronic demands. [1–4]. However, there are widespread concerns regarding the protection system against the occurrence of faults, particularly in poly-source distribution networks [5–7].

The advantage of the DC systems is high efficiency [6], power flow optimization [7,8] reduction of equipment size and weight [7], fewer converters requirements [6,7,9] and more power transfer capacity [8,9]. Ring-bus microgrids are one of the common structures of microgrids. It was shown that ring-bus microgrids are more efficient than, particularly when the distribution line is not long [10]. Fig. 1 demonstrates a perceptual scheme of a ring-bus LVDC microgrids systems.

Notwithstanding its remarkable merits, the protection of LVDC microgrids faces plenty of challenges, as well as there is no existence of a published standard, solution, or experience with this regard [7]. In the distribution network, the ability of accurate fault detection and location brings merits like quick repair, maintenance, and safety, which can decrease the power outages [6,11]. Load flow optimization, the increment of power quality, and the reductions in size and weight of equipment are the other merits of DC networks. The attendance of power electronic equipment controls current to a specified value in fault situations, which significantly makes it tough to detect faults and estimate its locations [11–13].

☆ This work was supported by the University of Zanjan, Iran.
* Corresponding author.
E-mail addresses: ali_abdali@znu.ac.ir (A. Abdali), kmazlumi@znu.ac.ir (K. Mazlumi), noroozian@znu.ac.ir (R. Noroozian).

https://doi.org/10.1016/j.asoc.2019.03.051
1568-4946/

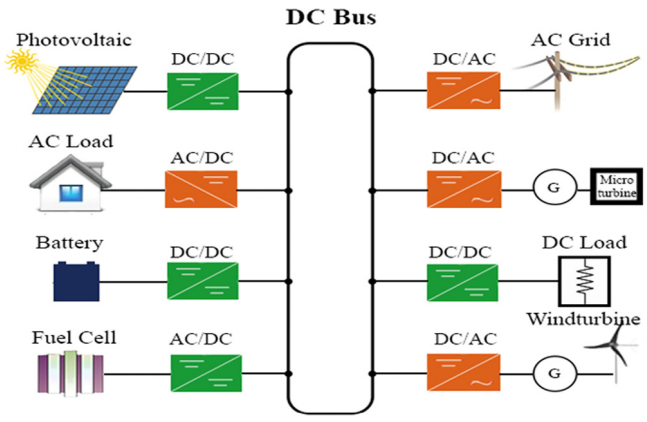

Fig. 1. Perceptual scheme of a ring-bus LVDC microgrids systems.

Generally, the protection methods of DC microgrid can be divided into unit protection and non-unit protection methods. The unit protection schemes are implemented to protect specific zones of a DC microgrid, for example, common DC bus, power electronic converters, energy storage devices like batteries or super capacitor banks, or loads, etc. In general, current deviations (according to the current law of Kirchhoff) are calculated in the specified zones of DC microgrids and the corresponding zone is only protected from fault. Example of this type is differential protection schemes [14–16].

Conversely, non-unit schemes basically follow a "threshold" value to detect the various faults. These schemes also protect the DC microgrid components without defining any specific zones. Therefore, these schemes can be used as a backup protection scheme for DC microgrids. Popular detection schemes under this category include: overcurrent, under/over-voltage, derivative of current (di/dt), the derivative of voltage (dv/dt) etc. [14–16].

In [17], it is demonstrated that the hierarchical protection and the localized differential scheme would provide effective protection schemes for the microgrids. Having wide area protection is the advantage of hierarchical protection scheme, but the disadvantage is that with the changes in microgrid system is inefficient because of short circuit levels change due to different circumstances, including microgrid islanding time, connecting the microgrid to the global network. But, the differential protection is efficient against the microgrid changes.

An event-based protection method for a hybrid DC power system has been presented in [18]. The suggested protection method offers less data transfer than common data-based protection, but the sub-transient short circuit current attains to multiple hundred amps during faults, which is disastrous to sensitive loads and power electronic equipment.

In [19,20] fast differential protection method for DC distribution networks has been proposed that is capable of detecting faults within millisecond faults. This method employed the natural properties of the DC differential current measurement to reduce the time of fault detection. The proposed method was applied and implemented in DC radial distribution systems and the protective device was installed at the beginning of each line. If this scheme is implemented on the ring-bus microgrid, protective devices were installed at the beginning and the end of each line. As a result, the relays should calculate the second derivative of the current both at the beginning and at the end of each line, and checks these two values together to detect the fault occurrence, which obviously will increase the fault detection time. So, if this scheme is implemented on the ring-bus microgrids, the fault detection time will be increased. In [21], a differential fault detection scheme in loop type LVDC microgrid was presented. This scheme utilized a determined threshold for fault detection. The major challenge of the differential protection method is hardness in choosing the threshold. However, the fault detection time of the differential scheme depends entirely on the selection of the threshold value. Increasing the value of the threshold enhance the fault detection time, which it is possible that either the faults will not be detected or the time of fault detection increases due to low fault current magnitudes. This value is determined based on the planners' and operators' experience. In Table 1, the summary of the recent literature review of DC protection schemes with methodology and the related description is stated.

In this paper, a new protection method based on the Multi-Criterion System (MCS) and Multi-Layer Perceptron (MLP) Neural Network (NN) for LVDC ring-bus microgrid systems are proposed. Indeed, the proposed protection system contains two parts: MCS and MLP NN protective systems. The MCS protective system is employed to high-speed fault detection in LVDC microgrids. In this section, all possible circumstance and cases for fault occurrence in whole sections of LVDC microgrids are extracted and appropriate decisions are taken to fault detection. Meanwhile, the MLP NN protective system is a backup and auxiliary system for the MCS protective system that estimates the location of the fault occurrence with high accuracy after the fault is detected. It is worth mentioning that the MPL NN protective system is integrated and coordinated with the MCS protective system. As a consequence, it can be stated that the contribution of the proposed method is as follows:

- The novel fast fault detection scheme in LVDC microgrids via MCS as a main protective system;
- Accurate fault location in LVDC microgrids via NN as a backup protective system for safety and maintenance considerations.

The first advantages of the present paper are that the protective algorithm does not depend on human actions and consideration and is fully intelligent, and secondly, the time of fault detection is decreased. First, a high-speed fault detection scheme via MCS is presented. Then, MLP NN is employed to estimate the fault location distance. Lastly, MCS and NN protection have been fulfilled and tested on a laboratory scale to evaluate the possibility and executable functionality of the presented methods.

2. The differential fault detection scheme

The type of faults, the accessible protection devices for DC systems, the differential fault detection scheme and its controller are noted in this section.

Two faults types could happen in DC microgrid. (1) Line-to-Line (LL) fault; and (2) Line-to-Ground (LG) fault. LG fault is the most prevalent type of fault in industrial distribution networks [26]. Due to restrictions of AC and Circuit Breakers (CB) in DC networks, a solid-state CB is opted for as a choice for DC protection. There are several choices, such as GTO, IGBT, and IGCT, which IGCTs present impressive and better efficiency [27–29]. A protective scheme for meshed DC microgrid systems was presented in [21]. A loop type DC bus was proposed to create a strong microgrid against fault circumstances. The meshed bus was separated into a series of sections. The presented protection system contains a master controller, two slave controllers and, freewheeling paths for each section. The master controller computes and monitors the difference between the input and output currents, whereas slave controllers are in charge of gauging of these current:

$$I_{diff} = I_{in} - I_{out} \tag{1}$$

Table 1
The summary of the recent literature review of DC protection schemes.

Reference	Type of protection scheme	Methodology	Description
[7]	Fault detection	Non-unit protection, Current based technique, Detect the fault via current, di/dt, and even d^2i/dt^2	In this paper, a protection system design based on circuit transient analysis and different protection devices for LVDC microgrids were proposed.
[8]	Fault detection and location	Non-unit protection, Current based technique, Detect the both LL and LG faults, discrete wavelet transform (DWT)	An accurate analysis of the wavelet-based scheme for fault detection and location in the HVDC network was provided in this paper. This paper tried to fully assess the overall efficiency of WT using real fault signals. The communication between the terminals has been eliminated because the wavelet detection method only needs a DC current signal that is attainable locally in each terminal.
[11]	Fault location	Current based technique, Estimate fault location with resistances of up to 2 Ω	A novel scheme for determining the location of the fault in the DC line via a Probe Power Unit (PPU) and a Fast Fourier Transform (FFT) was presented in this paper. This method does not need online current data to detect fault occurrence.
[18]	Fault classification	Unit protection, Event-based protection scheme, Sub-transient short circuit current technique, Low pass filter, Identify the type of fault	In this paper, an event-based protection method for a hybrid DC power system has been presented. The suggested protection method offers less data transfer than common data-based protection. Every protective system can automatically detect the event type via the current derivative fault classification method and artificial inductive line impedance. To precisely arrange the protection relays, the current analysis taking RC low pass filter effect into account were provided.
[20]	Fault detection and location	Unit differential protection, Current based technique, Estimate fault location with resistances of up to 2 Ω	In this paper, a novel current differential scheme for quick fault detection and location using Arc-Fault Circuit Interrupters (AFCI) as an auxiliary protective system in photovoltaic based DC microgrid has been presented.
[21]	Fault detection	Unit differential protection, Current based technique, Detect low impedance fault occurrence	In this paper, differential fault detection and isolation scheme by selecting a simple particular threshold value in loop type LVDC microgrid was presented.
[22]	Simultaneous control and fault detection	Control scheme: Developed suitable small signal model, Suitable control of power flow and cancellation of interactions Protection scheme: Unit protection, Current based technique, Detect low impedance fault occurrence	A new concurrent control and protection method for interconnected DC microgrid networks has been investigated in this paper. The presented control interface was based on a suitable small signal model for each DC microgrid and the proposed protection method is for quick detection of the fault in the DC link based on fuzzy logic.
[23]	Fault detection	Non-unit protection, Hybrid passive-overcurrent relay technique, Real-time discrete wavelet transform (DWT), Local-bus measurements, Detect low and high impedance (up to 200 Ω) fault occurrence	A hybrid passive overcurrent relay for the detection of high impedance faults in LVDC meshed grids was investigated in this paper. The proposed method was supplied with L and C to produces a particular recognized frequency under DC fault circumstance. The presented method employed both classical overcurrent functions and DWT to detect and recognize faults kinds with resistance up to 200 Ω. This scheme does not need communication between different buses.
[24]	Fault detection	Non-unit protection, Voltage and current based technique, Local intelligent electronic device (IED), Parameter estimation approach (Least Square (LS) based technique estimates)	Utilizing the local voltage and current information, the least squares-based method (LS) predicts the fault direction parameter that results from the fault was proposed in this paper. Utilizing the path of the fault data of both ends of a line section in a loop network, internal and external faults were detected to protect the network. Utilizing directional information for local faults, every IED recognizes any internal faults in the line section accurately.
[25]	Fault detection	Non-unit protection, Local measurements, Detect the fault through first and second derivatives transient fault current	Non-unit protection technique for DC microgrids utilizing only local measurements based on the natural properties of DC current and its first and second derivatives under fault transients was presented in this paper. Because of local measurements, communication lag challenges have been avoided.

Where 'I_{in}' and 'I_{out}' are input and output currents of each bus section. When the current difference (I_{diff}) value oversteps a threshold, the master controller recognizes it as a fault and handles the suitable considerations to the controllers. As mentioned earlier, the main drawback of this scheme is the utilization of the threshold for fault detection. This value is specified by the planner' experience and can clearly affect the speed of detecting and identifying the fault.

3. The proposed fault detection and location schemes using MCS and NN

The proposed fault detection and location based on MCS and NN are noted in this section. First MCS rules for fast fault detection are proposed, Then NN is applied to microgrid for fault location estimation.

Table 1 (*continued*).

Reference	Type of protection scheme	Methodology	Description
This paper	**Fault detection and location**	**Unit event-based protection, Data current based technique, Detect low and high impedance (up to 100 Ω) fault within a few milliseconds, Estimate low and high impedance fault location with low percent error**	**In this paper, a novel protection method based on Multi-Criterion System (MCS) and Multi-Layer Perceptron (MLP) Neural Network (NN) for loop type LVDC microgrid systems are proposed. Indeed, the presented protection system contains two parts: MCS and MLP NN protective systems. The MCS protective system is employed to fast fault detection in LVDC microgrids. In this section, all possible cases for fault occurrence in LVDC microgrids are extracted and appropriate decisions are taken to fault detection. Meanwhile, the MLP NN protective system is a backup and auxiliary system for the MCS protective system that estimates the location of the fault occurrence with high accuracy for safety and maintenance considerations.**

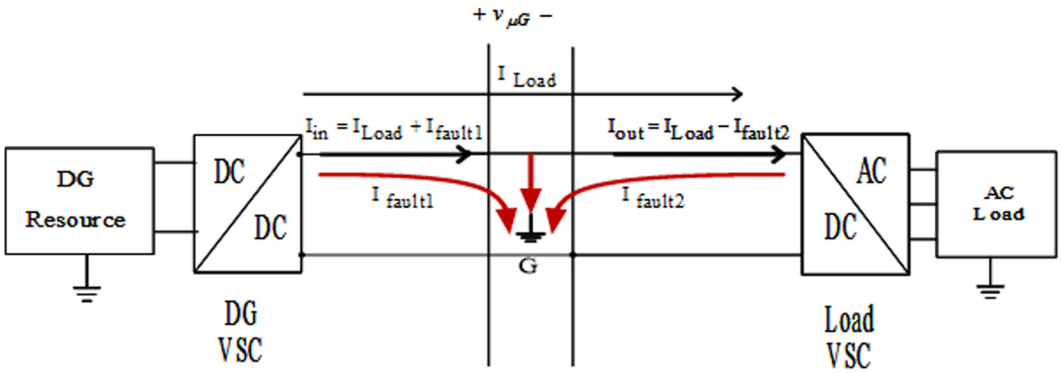

Fig. 2. The direction of current flow in faulted segA.

3.1. Fault detection scheme investigation in particular circumstance

A common bus is separated into different sections. Each section is monitored unendingly and its current is measured by two slave controllers. The rapidity and precision of master controller fault detection are strongly related to its capability to analyze data and fault detection methods. For instance, as far as Section 2 proposed method is concerned, it is clear that a fault is detected when a current difference between two sections passes beyond of threshold value; otherwise, no function has been done. Deem the following two instances:

(a) A high threshold value is set. (b) A low threshold value is set.

In the first case, if a high threshold value is selected, there is the likelihood that the current difference between the two sections does not overstep the specified threshold value in the fault circumstance. The magnitude of fault current depends on the network resistance and the fault current path. If the impedance of fault occurrence location is high or there is a large resistance in the fault current path, the maximum fault current reduces. Therefore, the master controller will not be able to detect high impedance faults.

In return, the threshold value for overcoming these problems can be decreased. Reduction of the threshold value will probably result in the wrong decision (relay wrong trip) by the master controller because of the power fluctuations or noise, while in fact, no fault has happened. Under such conditions, the low threshold value causes a reduction in the accuracy of fault detection. Pursuant to the above-mentioned descriptions, it is offered that another criterion, such as a connoisseur system, should be appended to the decision-making system. Based on particular MCS rules, MCS efforts to consider the most suitable and fastest decision for any state of the system. As a consequence, another yardstick for fault detection for loop type LVDC microgrids is presented in the next section. An MCS is then used as a substitute for the differential protection scheme, which can quickly detect faults.

3.2. Implementation of MCS as a new and expert controller for low impedance fault detection

To investigate and analyze the new criterion, assume that the fault happens in Segment A (segA) in Fig. 2. The input current to segA is computed as follows:

Where 'I_{fault1}' is the fault current entering the segA. The output current from the segA is specified as follows:

Output current from segA (I_{out}) = $I_{Load} - I_{fault2}$

Where 'I_{fault2}' is the fault current entering the segA. Fig. 2 indicates these currents. Considering the currents in segA, it can be deduced that in the fault circumstances in segA, the source side current goes up, since the fault current is gathered to the load current. Nonetheless, the load side current is reduced. In normal operation circumstances, while no fault has occurred, the current flow through the segA is equal at both the input and output of the segA. When a fault occurs in a segment such as segA, the current of input or output increases swiftly, which means that the rate of change is positive. At the same time, the current change rate on the other side is negative. The rules are classified that is fed into the MCS.

- If the fault occurs in a segment that contains a source (DG) and a DC static load:

Rule 1: IF I_{in} and I_{out} have the same values, THEN there was no fault has occurred.

Rule 2: IF I_{in} and I_{out} values are reducing, THEN there was no fault has occurred.

Rule 3: IF I_{in} and I_{out} values are increasing, THEN there was no fault has occurred.

Rule 4: IF I_{in} value is increasing and I_{out} value is reducing, $\frac{di_{in}}{dt} > 0$ & $\frac{di_{out}}{dt} < 0$, THEN a fault has occurred.

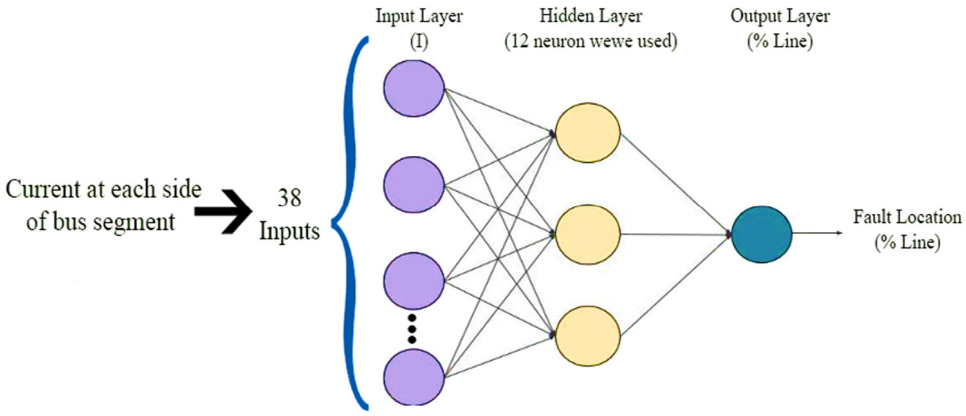

Fig. 3. 3-layer MLP feedforward NN.

Rule 5: IF I_{in} value is reducing and I_{out} value is increasing, $\frac{di_{in}}{dt} < 0$ & $\frac{di_{out}}{dt} > 0$, THEN a fault has occurred.
Rule 6: IF I_{in} and I_{out} are entering, THEN a fault has occurred.

• If the fault occurs in a segment that contains two sources:
Rule 7: IF I_{in} and I_{out} are entering and increasing, $\frac{di_{in}}{dt} > 0$ & $\frac{di_{out}}{dt} > 0$, THEN a fault has occurred.

• If a fault occurs in a zone that contains a source and an AC dynamic load (such as a motor):
Rule 8: Since the VSC-based DC/AC transform has the function of bi-directional energy transferring, the fault current can be provided by the load because of motor inertia and the interfacing converter's dc link capacitor discharges upon the fault occurrence. In this case, IF both I_{in} and I_{out} are entering and increasing to the relevant faulted segment, THEN a fault has occurred.

• If there is a fault in the segment that includes two loads (such as one DC static load and one AC dynamic load):
Rule 9: According to the previous rule, IF both I_{in} and I_{out} values are entering and increasing to the relevant faulted segment, THEN a fault has occurred.
Rule 10: If VSC is blocked because of hardware protection in the event of fault occurrence, the control signal is sent to the master controller with a change in the fault detection algorithm. IF both I_{in} and I_{out} values are reducing, THEN a fault has occurred and the faulted segment is isolated.

Rules 1 to 6 are considered as a rate of change of current criterion and current direction criterion. These criteria are demonstrated in Tables 2 and 3. The ✔ symbols *n* Tables 2 and 3 illustrates more significant outputs, which means that the fault must have occurred. These 10 rules help MCS to track currents in each section and make the most appropriate and precise determination based on the rate of change of current and current direction. The proposed MCS controller is the principal controller of loop type LVDC microgrids protection, and the differential method is considered as a backup and auxiliary protective system. MCS rules are carried out by the Fuzzy Inference System (FIS), and the type of employed FIS in this paper is Mamdani and has the following definition:

$$R_i: If\ x_1\ is\ \tilde{A}_{i1}\ and(or)\ x_2\ is\ \tilde{A}_{i2}\ and(or)\ \ldots x_m\ is\ \tilde{A}_{im}$$
$$Then\ y_i = \tilde{N}_i\ (i = 1, 2, \ldots, C) \quad (2)$$

The FIS rules are implemented by the 'AND' and 'OR' operators, and the Center of Gravity (COG) method is employed to specify the suitable output. Fuzzification and defuzzification of measured data (input and output currents of each section) are considered as triangular with equal distributions in an interval of $[-1, 1]$. In order to minimize errors in decision making, the number of successive cycles to corroborate the occurrence of the fault is considered in 3 cycles.

Table 2
The current directions criterion for low impedance fault detection.

I_{in} Direction	I_{out} Direction	Fault occurrence
Entering ↘	Exiting ↗	×
Exiting ↖	Entering ↙	×
Entering ↘	Entering ↙	✔

Table 3
The rate of current change criterion for low impedance fault detection.

I_{in}	I_{out}	Fault occurrence
0	0	×
Decreasing ↘	Decreasing ↘	×
Increasing ↗	Increasing ↗	×
Decreasing ↘	Increasing ↗	✔
Increasing ↗	Decreasing ↘	✔

3.3. Implementation of MLP NN

In this section, the objective is the fault location of the respective zone after fault detection. NNs are among the powerful and reliable approaches and are also used in many different engineering applications and problems to estimate promising results [30]. MLP NNs are able to make a nonlinear mapping with excellent accuracy via selection of the suitable number of layers and neural neurons, which is what we are seeking for. The amplitude of the fault current is inversely correlated with the impedance of the fault current path, i.e. if the impedance increases the fault current decreases and vice versa. Therefore, the relationship between the fault location and the fault impedance path can be expressed by a nonlinear mapping. Because the MLP NN performs nonlinear mappings with lower computational bulk and complexity, as well as with sufficient accuracy, the MLP neural network is used to estimate fault location.

3.3.1. Properties of NNs

Properties of NNs include adaptive training, self-organizing, real-time operators, fault tolerance, and, generalization [29]. MLP NNs are often formed by a number of single layers cascaded together, where the output of each layer is fed into the next. Each layer has a specific weight matrix '*w*', a bias vector '*b*', a net input vector '*n*', and an output vector '*a*'. A 3-layer feedforward MLP NN is demonstrated in Fig. 3. As can be seen, the number of inputs and neurons in the first layer of the 3-layer MLP feedforward NN are '*R*' and '*S*', respectively.

3.3.2. The selected structure based on NN

The selected structure of MLP is a 3-layer network, which has a lower computational bulk and complexity as well as sufficient accuracy in fault location estimation:

(a) Input layer: This layer is responsible for processing input signals to the NN, and uses interlayer coefficients to send output signals to the next layer. In this layer, the number of neurons and input variables are equal (I_{in} and I_{out}).

(b) Hidden layer: In this paper, to cover all possible states, the hyperbolic tangent transfer function is used in analyzing system conditions and making appropriate decisions accordingly. The neurons number in this layer may change, and the larger the number of neurons the more the processing power of the NN. There is always a trade-off between duration and computational costs, as well as the required accuracy. In this study, 12 neurons are considered for the hidden layer.

(c) Output layer: The processed data in the hidden layer is sent to the output layer after it is transformed into the appropriate commands and signals. In this paper, the hidden layer output is the length percentage of the transmission line, where a fault has occurred. A linear transfer function is used in this layer.

3.3.3. Training MLP NN

In order to train the NN for achieving suitable estimation accuracy, a database is first prepared. To this end, the microgrid in the previous section is simulated with different faults at different locations. Short circuit fault is applied to different line segments, from $d = 5\%$ to $d = 95\%$ (in steps of 5%) of the line length, and the corresponding fault currents are measured to be stored in a database matrix. Then the prepared database is used to train the NN. For the fault location using MLP NN, $\boldsymbol{I_{in}}$ and $\boldsymbol{I_{out}}$ currents are selected from each segment as a database. Then, it was used for offline training. The offline training of the MLP has carried out with the Error Back Propagation (EBP) method by the Levenberg–Marquardt (LM) algorithm. As well as, in the training epoch the number of iteration is considered 1000.

Significant attempts have been made to accelerate the EBP algorithm. All these methods cause to somewhat admissible results. The Levenberg–Marquardt (LM) algorithm follows the advancement of the EBP algorithm dependent methods [31,32]. This is a good exchange between the speed of Newton's algorithm and the durability of the fast descent method, which are two fundamental theorems of the LM algorithm [33].

The performance index $F(w)$ in the EBP method to be minimized is specified as the sum of the squares of the error among the objective outputs and the outputs of network simulation, i.e.:

$$F(w) = e^T e \tag{3}$$

Where $w = [w_1, w_2, \ldots, w_N]$ contains all weights of the network, e is the error vector comprising the error of whole the training samples. During training through the LM algorithm, the increment of weights Δw can be acquired as follows:

$$\Delta w = \left[J^T J + \mu I\right]^{-1} J^T e \tag{4}$$

In the above equation, J is the Jacobian matrix and μ is the learning rate that must be updated using β based on the result. Especially, μ is multiplied by the degradation rate $\beta (0 < \beta < 1)$ while $F(w)$ reduces, whilst μ is divided by β while $F(w)$ goes up in a new step. The pseudo-code of the standard LM training method can be shown in the following.

Pseudo-codes of LM algorithm

1. Weights and μ parameter initialization ($\mu = .01$ is suitable).
2. Sum of the squared errors over whole inputs $F(w)$ calculation.
3. In order to acquire the enhancement of weights Δw, solve (4).
4. Sum of squared errors $F(w)$ recalculation.

Utilizing $w + \Delta w$ as the trial w, and compare
IF trial $F(w) < F(w)$ in step 2 THEN
    $w = w + \Delta w$
    $\mu = \mu \cdot \beta (\beta = .1)$
    Return to step 2
ELSE
    $\mu = \mu / \beta$
    Return to step 4
END IF

4. Simulation results

The understudied LVDC microgrid is demonstrated in Fig. 4. The simulation circuit contains the exact model of wind turbine, exact model of photovoltaic cell, short line model with dispersed capacitors, freewheeling branches for fault current damping, bi-directional IGBT switches, antiparallel diodes of the IGBT switches, RCD snubber circuit to overcome voltages overshoot because of the line inductance impact, model of DC and AC loads, energy storage model, two-level VSC and DC/DC converters, the power electronics converters' DC link capacitors, VSC-based DC/AC converter, etc. Various segments are called as segA, segB, and segC. The voltages of DC supply sources in all segments are assumed to be 240 V, and the simulated network is TN grounded. Any section of the DC ring bus is 0.2 km cable and the network parameters are employed from [21,25]. The type of utilized snubbers is RCD. [34]. In the simulations, the delays of switching and communication were neglected but the effect of these delays has been considered in the practical implementation section.

4.1. Fault detection using MCS protection

The MCS-based protection system and understudied microgrid are simulated in MATLAB/ Simulink software. The kind of utilized solver is 'ode23tb (stiff/TR-BDF2)'. As well as, the employed sampling type is variable-step that the minimum step size is selected as the auto type and maximum step size is 10^{-4}. In order to compare MCS and differential fault detection methods, the MCS simulation situations are assumed alike with the differential scheme. As a result, LG short-circuit fault is applied to the center of segA (the section containing a source and a static DC load) at $t = 1$ ms and the utilized threshold value for differential protection method has been extracted from [16]. The evaluation of the simulation results demonstrates that the utilizing of the differential protection scheme in segA takes 250 μs to identify the fault occurrence and send a tripping command, while this value is 30 μs for an MCS controller. The high-speed performance with adequate precision is the certain merit of MCS protection against the differential protection method.

The input and output currents of the segA are demonstrated in Fig. 5. As can be seen, at the first instant, MCS and differential protection schemes experience the same current changes. Nevertheless, the MCS system swiftly detects a fault occurrence and sends a separation command. Whilst the differential protection scheme waits for the current difference to attain the utilized threshold value, causing a delay of 220 μs in tripping command. By utilizing the MCS intelligent protection scheme, much smaller current amounts can be experienced via fault currents, resulting in fewer detriment to the microgrid devices.

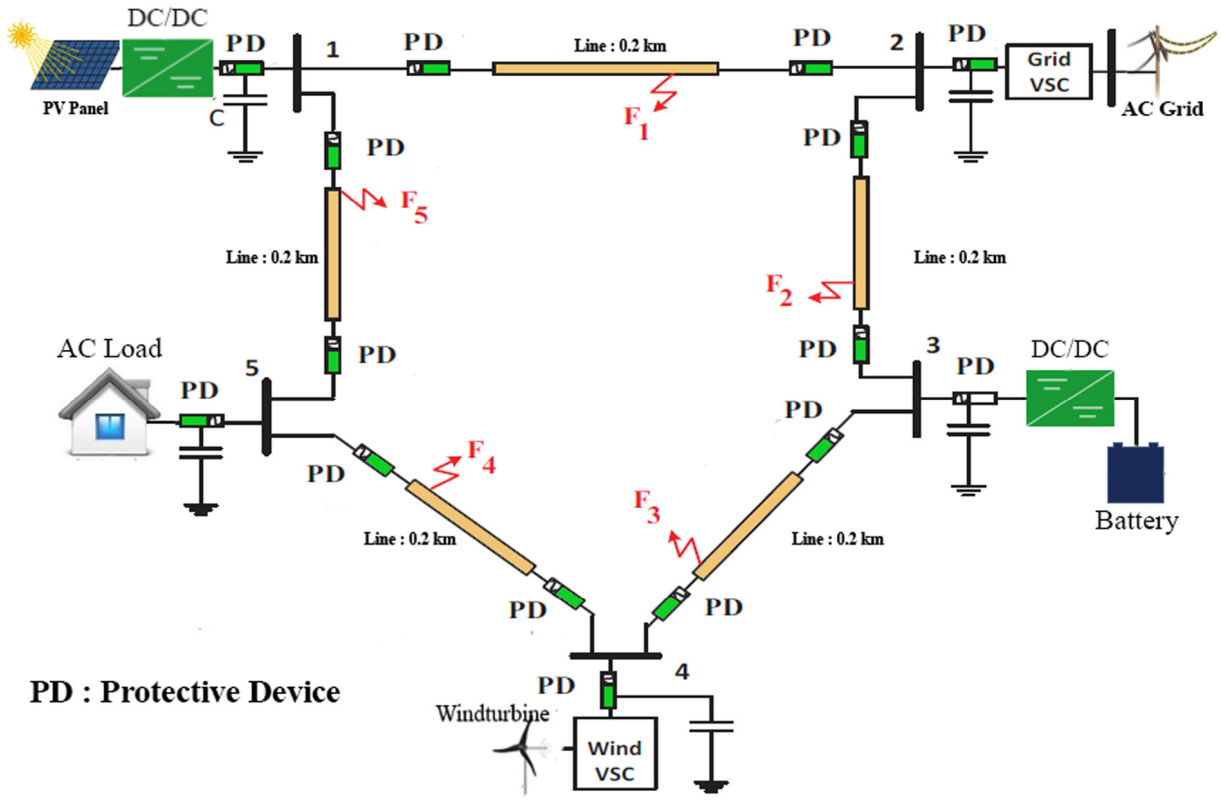

Fig. 4. LVDC ring-bus microgrid architecture considered in this study.

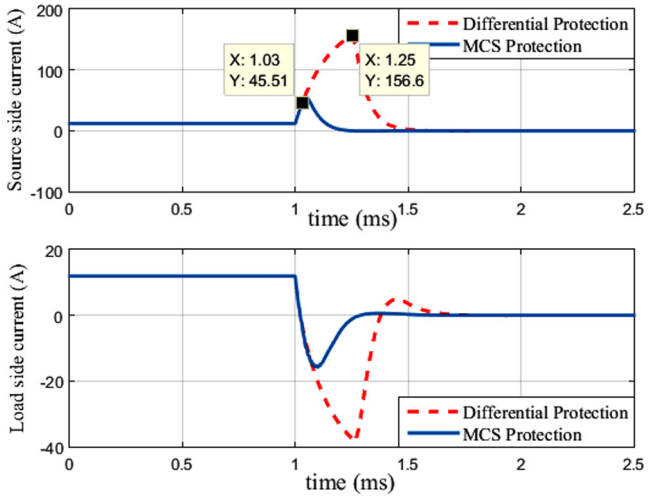

Fig. 5. The current of source side in segA (top) and Current of load side in segA (bottom) for low impedance LG short circuit.

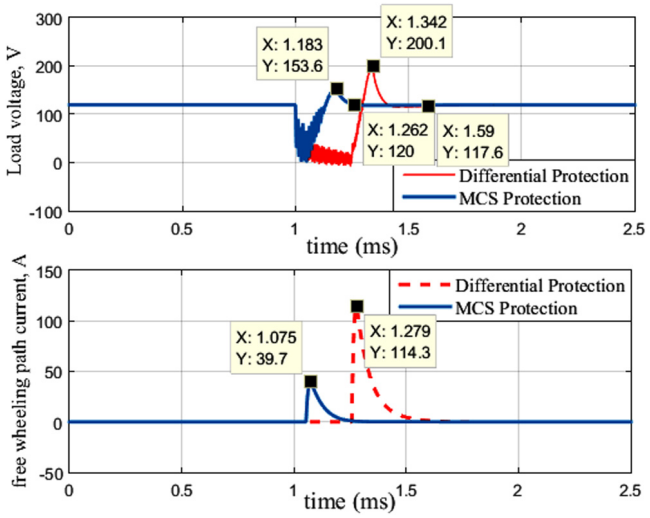

Fig. 6. The voltage of load in the presence of MCS scheme (top) and Flowing of fault current through diode freewheeling branch (bottom).

The load voltage in MCS and differential schemes is investigated in Fig. 6 (top). It is obvious, the MCS protection can restore the voltage and keep operation circumstances in normal case by high-speed fault detection and separation the corresponding faulted segment, while the differential scheme can only detect the fault occurrence and take the separation decision within the same period interval. The fault current flow in the diode freewheeling branch resulting from the MCS and differential schemes is compared and depicted in Fig. 6 (bottom). Utilizing the MCS protection scheme, high-speed fault detection and preventing an increase in fault currents, causes to flow smaller fault current in the freewheeling path compared to the differential protection scheme, which means lower cost of protection system and the possibility of the utilizing of simpler and smaller diodes with a lower price.

The voltage stress of the solid-state CB is demonstrated in Fig. 7. The utilizing of the MCS protection scheme reduces the maximum voltage stress on CB, which minimizes their installation costs and allows the employing of CB with lower rated insulation class. Exact simulation results are mentioned in Table 4.

Fig. 8 indicates the current of the source and load side in segA for the LG short circuit with 2.4 Ω fault resistance. As can be seen,

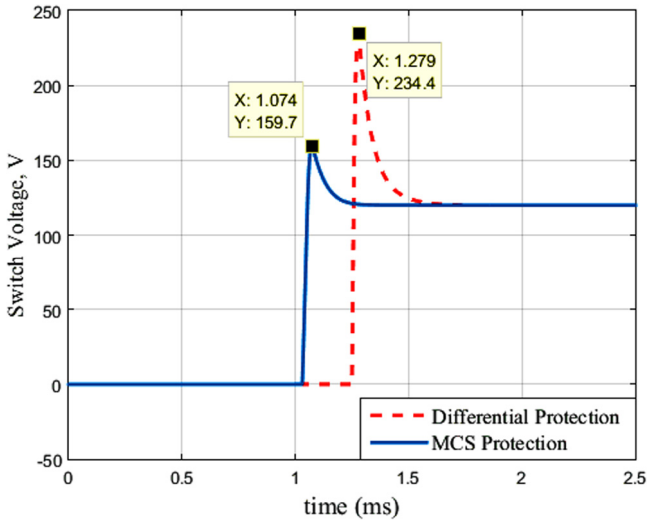

Fig. 7. CB voltage stress while segA is isolated.

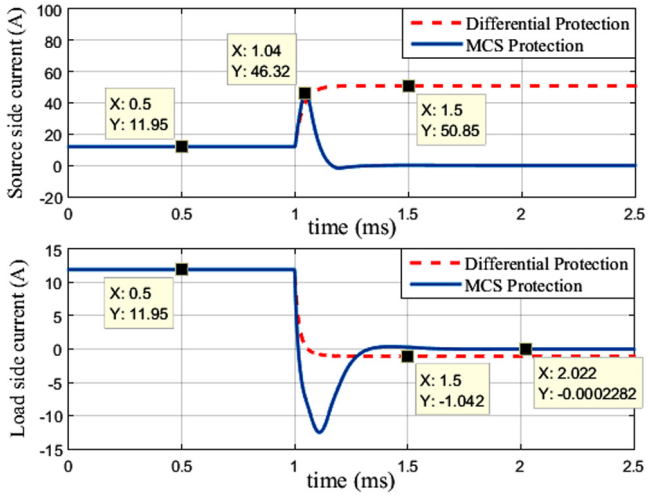

Fig. 8. The current of source side in segA (top) and Current of load side in segA (bottom) for LG fault with 2.4 Ω impedance.

Table 4
Simulation results report.

Items	MCS protection	Differential protection
Fault detection time	30 μs	250 μs
Load peak voltage (during fault occurrence)	153.6 V	200.1 V
Load voltage restoration time	262 μs	590 μs
Freewheeling path peak current (during fault occurrence)	39.7 A	114.3 A
CB peak voltage (during fault occurrence)	159.7 V	234.4 V

it is obvious that in this condition differential protection is unable to detect fault occurrence, but MCS protection as an expert and intelligent protection quickly predicts the fault occurrence after 40 μs in source side and sends an isolation command.

4.2. Fault location estimation using MLP NN

In this section, an MLP NN model is added to the microgrid simulation. The model uses the normal distribution function to normalize the input data. The normal distribution function is

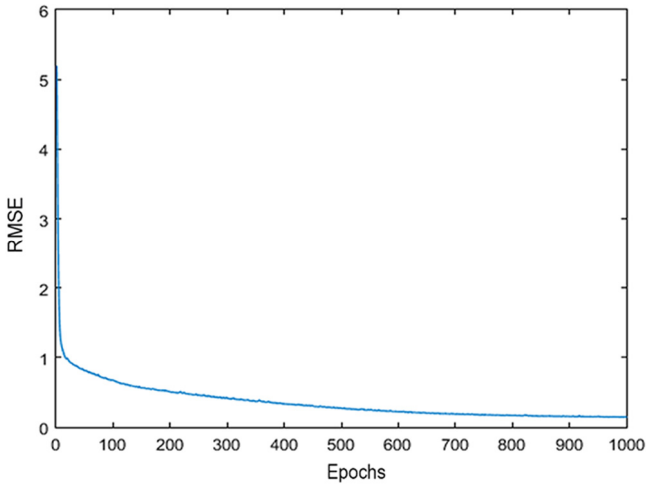

Fig. 9. Training algorithm convergence graph.

Table 5
Accuracy and validation results of assessing the MLP NN.

Epoch	Correlation coefficient	Maximum calculation error
Training	97.5%	5%
Test	98.3%	3.8%
Assessment	98.9%	1.6%

defined according to the mean value and variance of data as follows:

$$f\left(x.\mu.\sigma^2\right) = \frac{1}{\sigma\sqrt{2\pi}}\exp\left(-\frac{(x-\mu)^2}{2\sigma^2}\right) \tag{5}$$

After simulating the MLP NN, it is trained with the prepared database of different microgrid faults. Root Mean Square Error (RMSE) criterion is used to assess the training performance of the NN. The RMSE represents the error between real values from the database and the estimated values in each training epoch. In other words, the estimation error of all the data is equal to the RMSE percentage:

$$RMSE\% = 100 \times \sqrt{\frac{1}{N}\sum_{i=1}^{N}\left(y_i^{estimated} - y_i^{real}\right)^2} \tag{6}$$

Where N is the total number of training data. Smaller RMSE values mean higher accuracy of the NN in estimating objective function and the appropriate performance of the training process. Fig. 9 demonstrates the convergence graph of NN training.

As can be seen in Table 5, in the training epoch the correlation between the estimated values and real value is 97.5%, and the maximum error between them is 5%. Following the training epoch, no real values are provided to the NN, and outputs are estimated based on the input values. The test algorithm then updates NN weights according to the estimation error. In the next epoch, the NN is only assessed by receiving inputs that are not previously provided to the NN.

Then, the estimated outputs are assessed based on the corresponding inputs, but no weights are updated in this epoch. If the NN performance is not approved, training should be performed again from the beginning. The performance of NN in the assessment epoch is very promising. The MLP NN estimates fault location with a maximum error of 1.6%.

Simulated model of MLP neural network in "MATLAB/Simulink" software is demonstrated in Fig. 10. The detailed description of the neural network is as follows.

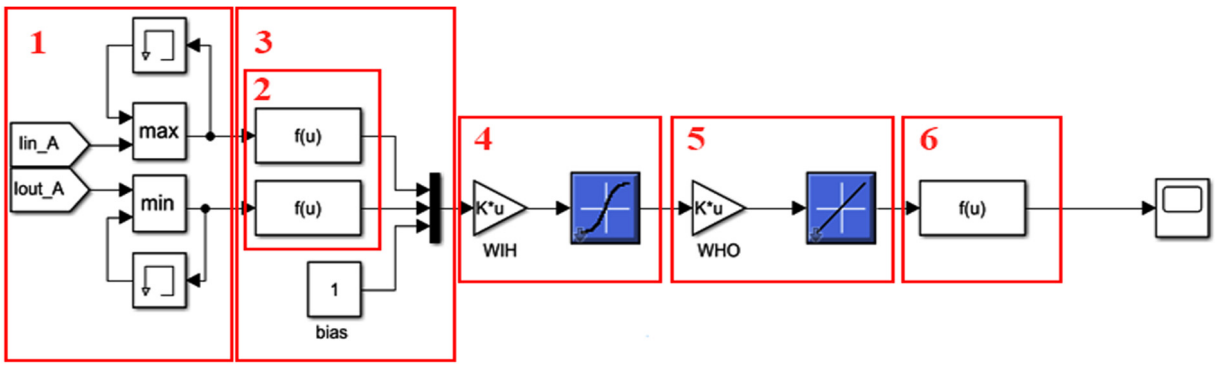

Fig. 10. Simulated model of MLP neural network in "MATLAB/Simulink" software.

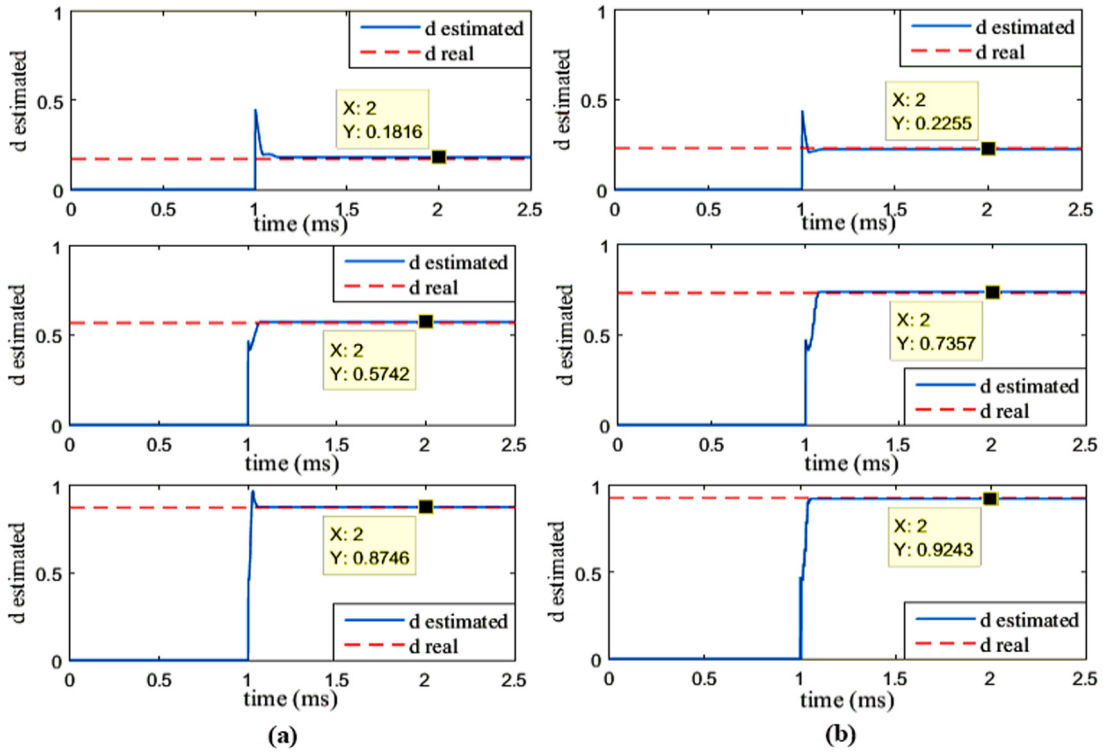

Fig. 11. Estimation of LL short circuit fault location in 17%, 57% and 87% of the line length (a) and estimation of LG short circuit fault location in 23%, 73% and 93% of the line length (b).

- Section 1: In this section, the input and output current of each section are measured at each instant and the maximum value is extracted by comparison with the pre-current value.
- Section 2: After the extraction of the maximum fault current in the two sides of the line (segment), data is normalized with the help of "$f(u)$" function. This function is written as a function in $f(u)$ blocks.
- Section 3: After the current values normalizing, along with the Bias, an NN input vector is formed.
- Section 4: By using the matrix multiplication in the Gain block, the coefficient weight matrix between the input and the hidden layer is multiplied to the input vector and the sigmoid tangent transfer function is applied to it.
- Section 5: The output of the hidden layer is multiplied to the weight matrix between the hidden layer and the output layer and passes through the linear transfer function. The output of this section is the estimated value of the NN.
- Section 6: The estimated value of the hidden layer is removed from the normal distribution space by the "$f(u)$" function and converted to the percent of line length.

For a better representation of NN capabilities, 6 different simulation results are demonstrated in Fig. 11. Fig. 11(a) demonstrates calculations of the fault location estimation for an LL fault occurring at 17%, 57% and 87% of the line length measured from the source side, respectively using the MLP NN. As can be seen from Fig. 11(a), the designed NN estimated the fault at 18.16%, 57.42% and 87.46% of the line length, respectively. The estimation errors for both states are calculated as 1.16%, 0.42%, and 0.46%.

Fig. 11(b) shows the estimation of the NN for an LG short circuit when the assumed fault is applied to a 46 m, 146 m and 186 m distance from the source side in segA, respectively. The designed NN estimated the fault at 22.55%, 73.57% and 92.43% of the line length, respectively. In other words, the MLP estimation was 45.1 m, 147.14 m and 184.86 m distance from the source side, respectively. The estimation error was calculated as 0.45%, 0.57% and 0.57% or 0.9m, 1.14m and 1.14m, respectively.

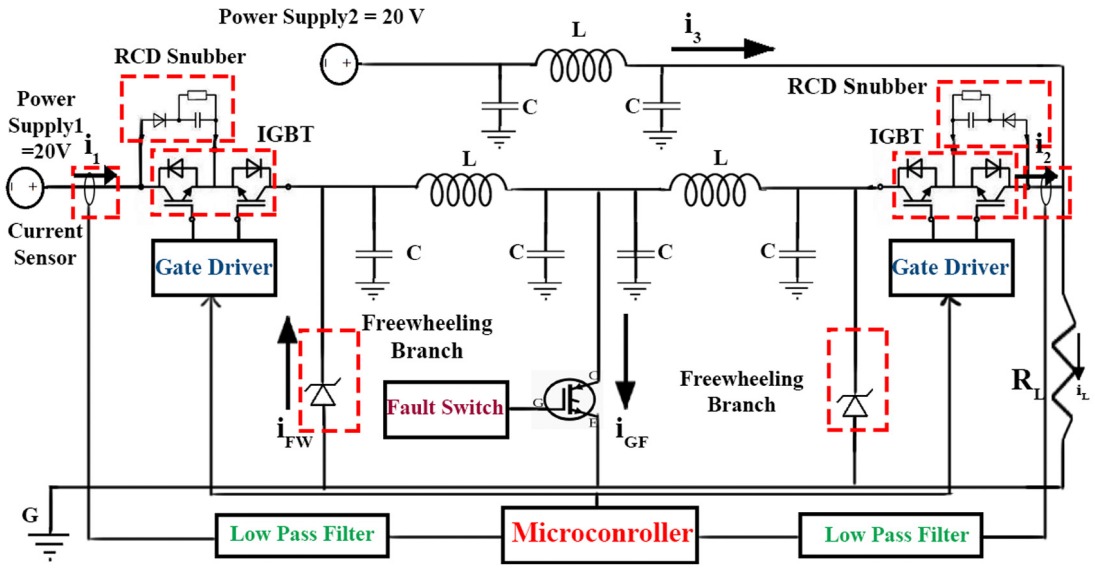

Fig. 12. Schematic of the experimental structure.

Table 6
Fault location estimation.

Fault distance in % of line length from the source (Fault type)	Fault distance from the source(m)	Distance estimation in % of line length	Distance estimation(m)	Estimation error
0.02 (LL)	4	0.0151	3.02	0.0049
0.08 (LG)	16	0.07912	15.824	0.00088
0.1 (LG)	20	0.09296	18.696	0.00702
0.19 (LL)	38	0.1989	39.78	0.0089
0.21 (LG)	42	0.2069	41.38	0.0031
0.26 (LL)	52	0.2599	51.98	0.0001
0.32 (LL)	64	0.313	62.6	0.007
0.38 (LG)	76	0.3843	76.86	0.0043
0.43 (LL)	86	0.4277	85.54	0.0023
0.49 (LG)	98	0.4871	97.42	0.0029
0.51 (LG)	102	0.5085	101.7	0.0015
0.56 (LL)	112	0.563	112.6	0.003
0.63 (LL)	126	0.6325	126.5	0.0025
0.66 (LG)	132	0.6615	132.3	0.0015
0.72 (LG)	144	0.7217	144.34	0.0017
0.79 (LL)	158	0.7926	158.52	0.0026
0.84 (LG)	168	0.8409	168.18	0.0009
0.88 (LL)	176	0.8863	177.26	0.0063
0.98 (LL)	196	0.9813	196.26	0.0013

For further assessment of the proposed MLP NN, Table 6 is provided. Table 6 is the result of fault location estimation using MLP NN for LG and LL short circuit. The results show that the estimation error is small and is within the permissible range. According to the results, efficiency and accuracy of MLP NN are confirmed.

5. Experimental validation

After performing numerical simulations, the question is that in the real scale networks are protection relay and CBs capable of rapid fault detection and isolation based on MCS? At the present time, because of the rapidity of analysis and decision-making of microcontrollers and also the high-speed power electronic equipment, it is envisaged that the presented method is enforceable and feasible. A 6:1 laboratory-scale practical setup is constructed from the simulation circuit to confirm the enforceability of the presented MCS scheme with the real hardware and equipment. The practical setup comprises a source-load-storage combination of Fig. 4, but the only the positive line (pole) is considered. Utilized devices, specifications, and related explanations are given in Table 7. The schematic of the practical setup structure is demonstrated in Fig. 12. The utilized DC voltage sources in the experimental setup are modeled as a two-channel power supply with a series resistance.

Also, in the implementation two-level VSC and DC/DC converters modeling is neglected and energy storage is modeled as a simple ideal source. The threshold value of the differential protection method is considered as 20% of the simulation threshold value. In this experiment, Analog-to-Digital (A/D) conversion of the measured current is carried out in 50 μs interrupt service routine. For fault location estimation, short circuit fault is applied to different line segments of the experimental setup, from $d =$ 10% to $d = 90\%$ (in steps of 10%) of the line length, and the corresponding fault currents are measured. Given the low number of database points, the hidden layers number is raised from 12 to 21 in order to achieve an acceptable accuracy in fault location estimation. Microcontroller and IGBTS gate drivers and practical experiment setup and utilized microcontroller are demonstrated in Figs. 13 and 14 respectively. Light LEDs of measured current modules demonstrates the valid connection among the current sensor and the microcontroller. An LG fault has been experimentally tested and applied in 1 s. In the normal steady-state

Table 7
Utilized devices and related explanations.

Equipment	Descriptions
Two-channels of 30-V 3-A power supply MASTECH HY3005-2	Implemented for 20-V source and energy storage
10 Ω, 30-Watt wire-wound resistor	Implemented for DC resistive load
Three 15 μH ferrite-core inductor	Implemented for line inductance
Six 220 pF ceramic capacitor	Implemented for stray capacitance
Two IGBT STGW38IH130D modules	Implemented for considering a bidirectional solid-state CB
One IGBT IKW40N120H3	Implemented for applying the LG fault
Diode FEP30GP, 2Ω wire-wound resistor	Implemented for freewheeling branches
Diode FEP30GP, 10 μF electrolytic capacitor, 12Ω resistor	Implemented for RCD snubbers
ATMEGA8L-8PU Microcontroller	Implemented for the fault detection scheme
Three ACS 712-30 measurement current modules	Implemented for sampling current, a 3rd order Low-Pass Filter (LPF), Analog-to-Digital (A/D) converter
Three TC427CPA microchips, ULN2003 APC buffer	Implemented for IGBTs gate drivers The IGBTs gate drivers are accomplished in the Darlington pair for synchronous performance of the IGBT switches
Two HCPL-7840 optocoupler	Implemented for isolation of analog ground from digital ground, noise decrement

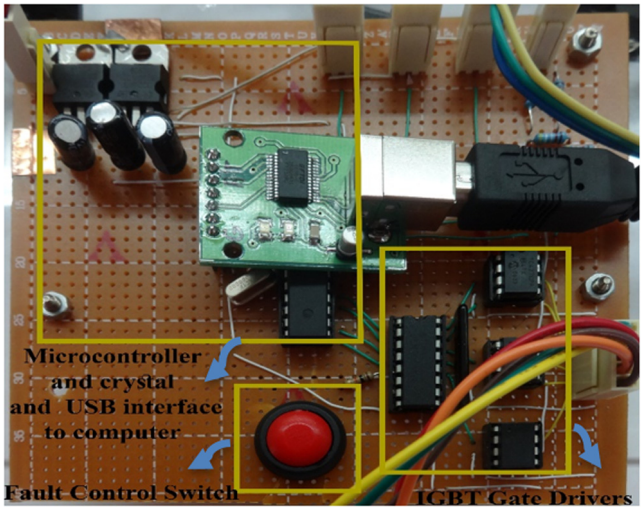

Fig. 13. Microcontroller and IGBTS gate drivers.

circumstance, the source supplies 20 W (20V, 1A) to the load. When an LG fault occurs, two-channel power supply feeds the fault current and segment sensors measure the currents. It should be noted that the power supply can supply about 20 A peak transient fault current for 100 ms before each channel reaches a 3A nominal current value. As a result, without protection laboratory waveforms, and without protection simulated waveforms will be different.

Fig. 15 shows the source and load side current without protection, differential, and MCS protection. Without protection, a 6 A fault current flows after the transient. But by comparing MCS and differential algorithm waveforms it can be concluded that MCS protection can detect fault occurrence in less time. As can be seen, after isolation the current value reaches zero.

Fig. 16 depicts the load voltage and the current flowing freewheeling path without protection, differential, and MCS protection. As can be seen, the load voltage with MCS protection is restored more quickly and possesses fewer transient. Without protection, the load voltage reaches a small amount. Utilizing the MCS protection scheme, high-speed fault detection and preventing an increase in fault currents, causes to flow smaller fault current in the freewheeling branch compared to the differential protection scheme, which means lower cost of protection system and the possibility of the utilizing of simpler and smaller diodes with a lower price.

Table 8
Experimental validation results report.

Items	MCS protection	Differential protection
Fault detection time	19 ms	87 ms
Load peak voltage (during fault occurrence)	26.38 V	35.35 V
Load voltage restoration time	185 ms	275 ms
Freewheeling path peak current (during fault occurrence)	2.766 A	7.523 A
CB peak voltage (during fault occurrence)	89.88 V	188.1 V

The voltage stress of the solid-state CB in presence of snubber is demonstrated in Fig. 7. The utilizing of the MCS protection scheme reduces the maximum voltage stress on CB, which minimizes their installation costs and allows the employing of CB with lower rated insulation class. As well as, by utilizing the MCS scheme, IGBTs experienced fewer transient and in this state, the possibility of destruction of CB is reduced.

As can be seen, by the implementation MCS protection algorithms and corresponding tests, it can be concluded that MCS method is applicable, and the feasibility and efficiency, rapidity and accuracy of the algorithm are shown compared to the differential method. In the simulation section, the delays of switching and communications were not considered, as a result, faults are detected in the microseconds. But in this practical implementation network, due to the delays of switching and communications, faults are detected in milliseconds, which seems logical. A detailed report of the experimental validation results is presented in Table 8.

As we know, in the operation of energy transmission systems, the size and capacity of the equipment are selected based on the voltage and current that can be tolerated, and the price of the equipment is directly related to the amount of voltage and current it can tolerate. For example, solid-state IGBT that tolerates a voltage of 100 V and a current of 150 A, it is more expensive than the IGBT that tolerates a voltage of 75 V and a current of 100 A. It is also clear that if the protection system can detect faults as quickly as possible, equipment will tolerate less voltage and less current flow. By using the MCS protective system, equipment experiences much smaller fault currents values, result in fewer damage to the microgrid devices and consequently decrease system protection and operation costs. For example, as shown in Fig. 14, the current flowing through the IGBTs in the fault occurrence by using the MCS protection method is ultimately 8.5 A, while by the use of differential protection method is 18.3 A

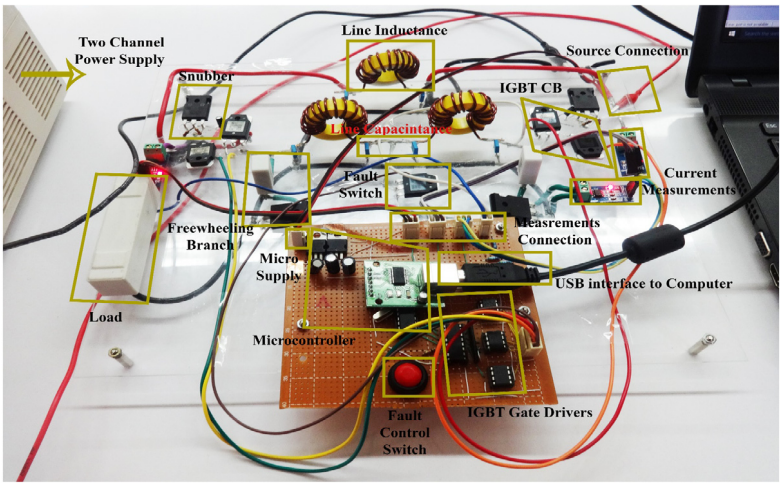

Fig. 14. Practical experiment setup and utilized microcontroller.

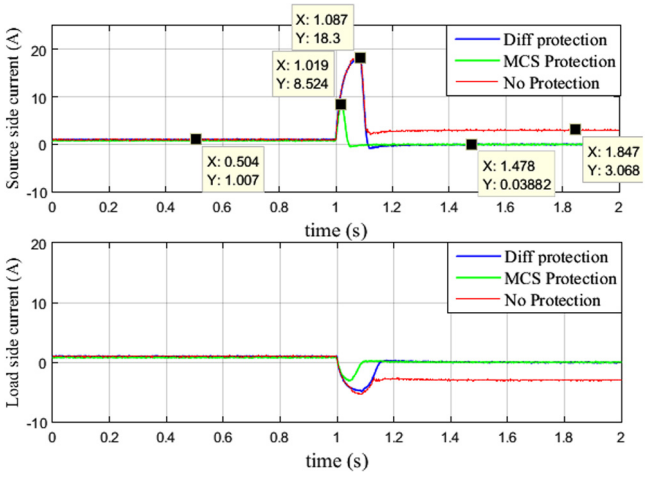

Fig. 15. Source and load side current for without protection, differential, and MCS protection.

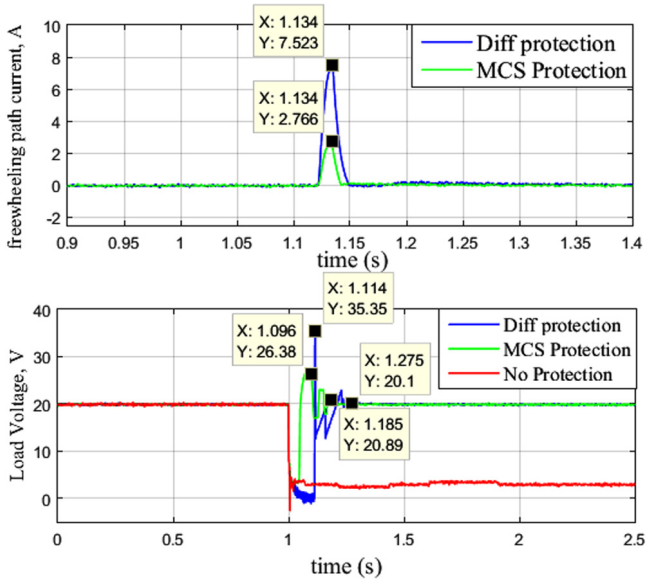

Fig. 16. Load voltage and the current flowing freewheeling path without protection, differential, and MCS protection.

(more than twice). The voltages of IGBTs and snubber circuit by using the MCS protection method is 90 V, while by the use of differential protection is 188 V (more than twice). As a result, by using the MCS protective system, it can be used with less capacity equipment that consequently decreases system protection and operation costs.

Fig. 18 (top) demonstrates the calculation of the fault location estimation for an LG fault occurring at 40% of the line length measured from the source side using the MLP NN. As can be seen, the designed NN estimated the fault at 40.46% of the line length. The estimation error is calculated as 0.46% or 0.92 m. Fig. 17 (bottom) demonstrates the calculation of the fault location estimation for an LG fault occurring at 82% of the line length measured from the source side using the MLP NN. As can be seen, the designed NN estimated the fault at 82.38% of the line length. The estimation error is calculated as 0.38% or 0.76 m. As can be seen, despite the high noise in the laboratory setup, the designed NN can estimate the fault location in the acceptable range.

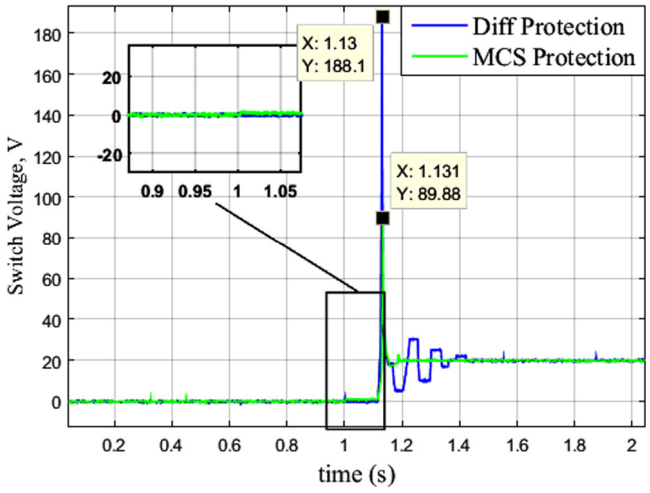

Fig. 17. CB voltage stress in the presence of snubber with differential, and MCS protection.

6. Conclusion

This paper presents new fault detection and location schemes for loop type LVDC microgrids systems. The proposed protection method is based on MCS and NN and contains expert and flexible

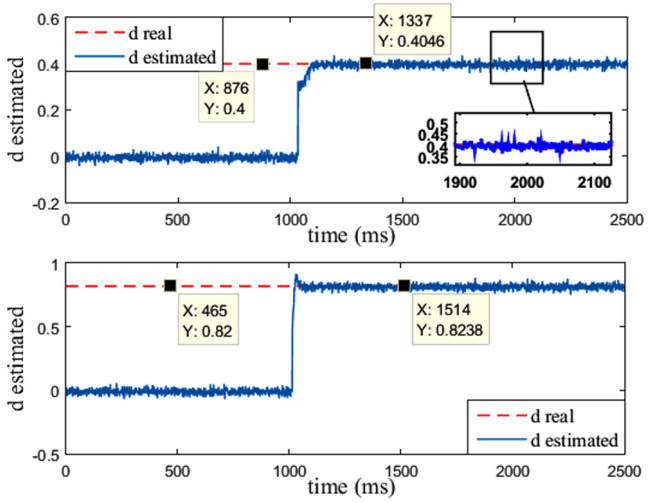

Fig. 18. Estimation of LG short circuit fault location in 40% of the line length(top) and estimation of LL short circuit fault location in 82% of the line length(bottom).

controllers that can detect faults faster than other available methods. Results demonstrate the precision and efficiency of the fault location method based on MLP NN. High-speed fault detection is the merit of the MCS, which decreases protection system costs and makes it possible to utilize devices with lower insulation. As well as, with the implementation of MCS and NN protection schemes, it can be deduced that these methods are feasible and the enforceability, efficiency, rapidity, precision of the proposed methods are depicted in comparison with the differential method. The proposed schemes could be implemented in various LVDC networks.

Conflict of interest

No author associated with this paper has disclosed any potential or pertinent conflicts which may be perceived to have impending conflict with this work. For full disclosure statements refer to https://doi.org/10.1016/j.asoc.2019.03.051.

References

[1] Y.M. Yeap, N. Geddada, A. Ukil, Analysis and validation of wavelet transform based dc fault detection in hvdc system, Appl. Soft Comput. 61 (2017) 17–29.
[2] W.J. Ma, J. Wang, X. Lu, V. Gupta, Optimal operation mode selection for a dc microgrid, IEEE Trans. Smart Grid 7 (6) (2016) 2624–2632.
[3] M.T. Benchouia, I. Ghadbane, A. Golea, K. Srairi, M.E.H. Benbouzid, Implementation of adaptive fuzzy logic and pi controllers to regulate the dc bus voltage of shunt active power filter, Appl. Soft Comput. 28 (2015) 125–131.
[4] M.J. Sanjari, H. Karami, A.H. Yatim, G.B. Gharehpetian, Application of hyper-spherical search algorithm for optimal energy resources dispatch in residential microgrids, Appl. Soft Comput. 37 (2015) 15–23.
[5] L.L. Li, G.Q. Lin, M.L. Tseng, K. Tan, M.K. Lim, A maximum power point tracking method for pv system with improved gravitational search algorithm, Appl. Soft Comput. 65 (2018) 333–348.
[6] M.D. Cook, G.G. Parker, R.D. Robinett, W.W. Weaver, Decentralized mode-adaptive guidance and control for dc microgrid, IEEE Trans. Power Deliv. 32 (1) (2017) 263–271.
[7] D. Salomonsson, L. Soder, A. Sannino, Protection of low-voltage dc microgrids, IEEE Trans. Power Deliv. 24 (3) (2009) 1045–1053.
[8] S. Mirsaeidi, X. Dong, S. Shi, D. Tzelepis, Challenges, advances and future directions in protection of hybrid ac/dc microgrids, IET Renew. Power Gener. 11 (12) (2017) 1495–1502.
[9] S.P. Azad, R. Iravani, J.E. Tate, Stability enhancement of a dc-segmented ac power system, IEEE Trans. Power Deliv. 30 (2) (2015) 737–745.
[10] M. Saisho, T. Ise, K. Tsuji, Configuration of DC loop type quality control center, in: Power Conversion Conference, 2002. PCC-Osaka 2002. Proceedings of the IEEE, vol. 2, 2002, pp. 434–439.
[11] R. Mohanty, U.S.M. Balaji, A.K. Pradhan, An accurate noniterative fault-location technique for low-voltage dc microgrid, IEEE Trans. Power Deliv. 31 (2) (2016) 475–481.
[12] A. Abdali, K. Mazlumi, R. Noroozian, A precise fault location scheme for low-voltage dc microgrids systems using multi-layer perceptron neural network, Sigma J. Eng. Nat. Sci. 36 (3) (2018) 821–834.
[13] A. Abdali, K. Mazlumi, R. Noroozian, Fast fault detection and isolation in low-voltage dc microgrids using fuzzy inference system, in: 5th Iranian Joint Congress on Fuzzy and Intelligent Systems (CFIS), Qazvin, 2017, IEEE, 2017, pp. 172–177, http://dx.doi.org/10.1109/CFIS.2017.8003678.
[14] A. Hooshyar, R. Iravani, Microgrid protection, Proc. IEEE 105 (7) (2017) 1332–1353.
[15] S. Augustine, J.E. Quiroz, M.J. Reno, S. Brahma, DC Microgrid Protection: Review and Challenges.
[16] L. Zhang, T.A.I. Nengling, W. Huang, L.I.U. Jian, W.A.N.G. Yanhong, A review on protection of dc microgrids, J. Mod. Power Syst. Clean Energy (2018) 1–15.
[17] L. Che, M.E. Khodayar, M. Shahidehpour, Adaptive protection system for microgrids: protection practices of a functional microgrid system, IEEE Electrific. Mag. 2 (1) (2014) 66–80.
[18] M. Farhadi, O.A. Mohammed, Event-based protection scheme for a multiterminal hybrid dc power system, IEEE Trans. Smart Grid 6 (4) (2015) 1658–1669.
[19] S.D. Fletcher, P.J. Norman, K. Fong, S.J. Galloway, G.M. Burt, High-speed differential protection for smart dc distribution systems, IEEE Trans. Smart Grid 5 (5) (2014) 2610–2617.
[20] S. Dhar, R.K. Patnaik, P.K. Dash, Fault detection and location of photovoltaic based dc microgrid using differential protection strategy, IEEE Trans. Smart Grid 9 (5) (2018) 4303–4312.
[21] J.D. Park, J. Candelaria, Fault detection and isolation in low-voltage dc-bus microgrid system, IEEE Trans. Power Del. 28 (2) (2013) 779–787.
[22] A. Abdali, R. Noroozian, K. Mazlumi, Simultaneous control and protection schemes for dc multi microgrids systems, Int. J. Electr. Power Energy Syst. 104 (2019) 230–245, http://dx.doi.org/10.1016/j.ijepes.2018.06.054.
[23] K.A. Saleh, A. Hooshyar, E.F. El-Saadany, Hybrid passive-overcurrent relay for detection of faults in low-voltage dc grids, IEEE Trans. Smart Grid 8 (3) (2017) 1129–1138.
[24] R. Mohanty, A.K. Pradhan, Protection of smart dc microgrid with ring configuration using parameter estimation approach, IEEE Trans. Smart Grid (2017).
[25] A. Meghwani, S.C. Srivastava, S. Chakrabarti, A non-unit protection scheme for dc microgrid based on local measurements, IEEE Trans. Power Deliv. 32 (1) (2017) 172–181.
[26] J.C. Das, R.H. Osman, Grounding of ac and dc low-voltage and medium-voltage drive systems, IEEE Trans. Ind. Appl. 34 (1) (1998) 205–216.
[27] J.B.L. Fermeiro, J.A.N. Pombo, M.R.A. Calado, S.J.P.S. Mariano, A new controller for dc-dc converters based on particle swarm optimization, Appl. Soft Comput. 52 (2017) 418–434.
[28] X. Ding, M. Du, T. Zhou, H. Guo, C. Zhang, Comprehensive comparison between silicon carbide mosfets and silicon igbts based traction systems for electric vehicles, Appl. Energy 194 (2017) 626–634.
[29] P. Steimer, O. Apeldoorn, E. Carroll, A. Nagei, IGCT technology baseline and future opportunities, in: IEEE PES Transmission and Distribution Conference and Exposition, vol. 2, 2001 pp. 1182–1182.
[30] L.V. Fausett, Fundamentals of Neural Networks: Architectures, Algorithms, and Applications, vol. 3, Prentice-Hall, Englewood Cliffs, 1994.
[31] M.T. Hagan, M.B. Menhaj, Training feedforward networks with the marquardt algorithm, IEEE Trans. Neural Netw. 5 (6) (1994) 989–993.
[32] N. Leema, H.K. Nehemiah, A. Kannan, Neural network classifier optimization using differential evolution with global information and back propagation algorithm for clinical datasets, Appl. Soft Comput. 49 (2016) 834–844.
[33] R. Battiti, First-and second-order methods for learning: between steepest descent and newton's method, Neural Comput. 4 (2) (1992) 141–166.
[34] S.Y. Lin, C.L. Chen, Analysis and design for RCD clamped snubber used in output rectifier of phase-shift full-bridge ZVS converters, IEEE Trans. Ind. Electron. 45 (2) (1998) 358–359.